applied sciences

MDPI

Article

Design Method and Mechanical Behavior of Modular Composite Steel Temporary Bridges on Soft Paddy Field Foundations

Dongrui Song [1], Zhongzheng Cui [2], Zhaoqing Chen [2,*], Dong Han [1], Yanyang Bai [1] and Zhongfeng Kan [1]

[1] Jilin Power Supply Company, State Grid Jilin Electric Power Co., Ltd., Jilin 132011, China
[2] School of Civil Engineering and Architecture, Northeast Electric Power University, Jilin 132012, China
* Correspondence: chenzhq2004@neepu.edu.cn

Abstract

To address the challenges of low bearing capacity in Northeast China's paddy-field soft foundations and the limitations of summer power line construction, a standardized design method for a novel prefabricated modular steel temporary bridge is proposed. Based on the Winkler elastic foundation beam theory, the operating characteristics of rigid short beams and the subgrade reaction distribution under heavy loads were analyzed. On this basis, combined with in situ static load tests and finite element analysis (FEA), the mechanical performance of the temporary bridge under the static loads of crawler-type and six-wheel construction machinery was investigated. The results indicate that when the bridge deck is subjected to a 25-ton construction vehicle, the maximum stress and displacement in the mid-span condition remain well below the material yield strength and the allowable limits stipulated in the *Specifications for Design of Highway Steel Bridges* (JTG D64-2015). Furthermore, the temporary bridge structure maintains excellent operational stability under a 100-ton extreme construction load and eccentric loading conditions. This study elucidates the mechanical behavior of the temporary bridge, providing a scientific theoretical basis and engineering reference for the design of temporary transit structures in complex environments such as soft paddy field foundations.

Keywords: portable bridge; steel structure; static analysis; mechanical performance; numerical simulation

1. Introduction

Prefabricated temporary steel structures play an irreplaceable role in emergency infrastructure construction and traffic transit through complex environments due to their distinct advantages, including standardized design, rapid on-site assembly, and high turnover rates. In recent years, with the promotion of Accelerated Bridge Construction (ABC) philosophies [1], the demand for modular steel bridge systems featuring high load-bearing capacity and superior environmental adaptability has risen sharply. However, conventional prefabricated temporary bridges mostly use classic truss systems, such as Bailey bridges [2]. Although these structures exhibit excellent extensibility when spanning spatial obstacles like deep valleys and rivers, they present obvious limitations in flat yet extremely weak foundation environments.

Using power line construction during summer in Northeast China as a case study, the vast fields are always waterlogged, forming ultra-weak elastic–plastic foundations characterized by fluid–plastic or soft–plastic behaviors. Traditional methods—such as thick subgrade laying, deep cement mixing, or concrete cofferdams—not only require lengthy

Check for updates

Academic Editor: Asterios Bakolas

Received: 4 June 2026
Revised: 5 July 2026
Accepted: 7 July 2026
Published: 15 July 2026

Copyright: © 2026 by the authors. Licensee MDPI, Basel, Switzerland. This article is an open access article distributed under the terms and conditions of the Creative Commons Attribution (CC BY) license.

construction periods but also involve extensive on-site wet operations that severely disturb and permanently damage the fragile agricultural paddy ecology. Therefore, it is highly urgent to develop a novel plate–beam composite prefabricated load-transfer system. Such a system must effectively disperse the extreme concentrated loads of heavy construction vehicles, adapt to the settlement deformations of ultra-weak foundations, and ensure exceptionally high structural safety.

To address the structural response of temporary bridge systems under non-ideal boundary conditions, researchers worldwide have recently conducted extensive cutting-edge investigations using digital simulations and full-scale experiments. Regarding the evaluation of the mechanical performance of prefabricated bridge components and joints, Embaby et al. [3,4] thoroughly analyzed the stiffness evolution and load-transfer mechanisms of modular double-truss bridges and steel shear wall panels under static and dynamic loads. Luo et al. [5] explored seismic performance prediction and surrogate models under vehicle–bridge coupling effects. Bao et al. [6] further quantified the ultimate compressive and bearing design boundaries of steel main girders. However, most of these advanced studies simplify the structural support boundaries into absolutely rigid supports or continuous elastic foundations with constant stiffness, leaving a critical gap in coupled analyses explicitly targeting waterlogged, fluid–plastic soft paddy foundations.

Empirical data from field testing accurately capture the actual structural performance of bridges, providing essential validation for design, construction control, and safe operation. Khounsida et al. [7] experimentally analyzed the static and dynamic behavior of an in-service Bailey bridge, demonstrating that structural weakening can be attributed to complex transverse and vertical vibration modes. Kusimba et al. [8] installed displacement sensors on a Bailey bridge in Japan and measured the maximum compressive stress at the top chord of the center panel. Yi et al. [9] conducted a load-rating assessment of a 55 m span Bailey bridge using T44 truck loads, examining its performance under various military load classifications through structural analysis. Biondini and Malerba [10] systematically studied the structural collapse mechanisms of existing Bailey bridges, showing that structural failure is primarily triggered by secondary stresses induced by out-of-plane deformations.

During the preliminary design stage of temporary bridges, finite element modeling serves as an effective validation tool [11]. Embaby et al. [4] conducted experimental and finite element analyses on steel truss shear panels of Bailey bridges to propose an effective length factor that modifies the AASHTO code [12], significantly enhancing the calculation accuracy of load-bearing capacity from 61.6% to 95.4%, thereby resolving the over-conservatism of the original specification. However, this represents a fully idealized state that is difficult to apply directly to complex field conditions. Tong Wu et al. [13] used numerical simulation methods to study the mechanical response and failure mechanisms of shallow-foundation bridges under the coupled actions of flood scouring and heavy vehicle loads, focusing on the bearing capacity variations and ultimate failure modes of the foundation after soil loss. Liang Luo et al. [5] simulated the seismic performance prediction and interpretation of RC bridges under vehicle–bridge interaction, demonstrating the seismic behavior of bridges under moving loads. Wang et al. [14] thoroughly investigated deformation-induced fatigue cracking performance at the web gaps of multi-girder steel bridges under vehicle loads. Shi et al. [15] investigated the overturning failure mechanism of girder bridges based on finite element simulations and simplified calculation methods, indicating that overturning failure is driven not only by global instability but also by the strength failure of individual components. Xiong et al. [16] systematically studied the overturning collapse problem of girder bridges using static finite element methods, establishing a quantitative evaluation framework that divides the overturning process into four intermediate limit states using bearing reaction forces and main girder rotation

angles as key parameters. Finite element simulation has clearly become a necessary step in modern bridge design.

Prefabricated temporary bridges [17] represent an effective technological pathway to resolve summer transit challenges in paddy field construction. By adopting standardized designs, factory prefabrication, and modular assembly, they significantly enhance construction efficiency, guarantee structural safety, and reduce ecological disturbances to the paddy environment. In alignment with current green construction philosophies, paddy field operations must minimize damage to the natural ecology. Concrete temporary bridges [18] are less applicable to such projects due to their extensive on-site wet operations, non-recyclable materials, and severe foundation disturbances. Furthermore, because transmission line construction requires the frequent passage of large-scale mechanical equipment, the load-bearing capacity of the temporary bridge stands as the core design consideration; it must satisfy the transit safety and operational stability of heavy vehicles such as concrete mixers and crawler cranes. Compared with other structural forms, steel temporary bridges [6] leverage high strength, lightweight attributes, and exceptional mechanical performance to better satisfy these heavy load demands, making them the ideal choice for this application scenario.

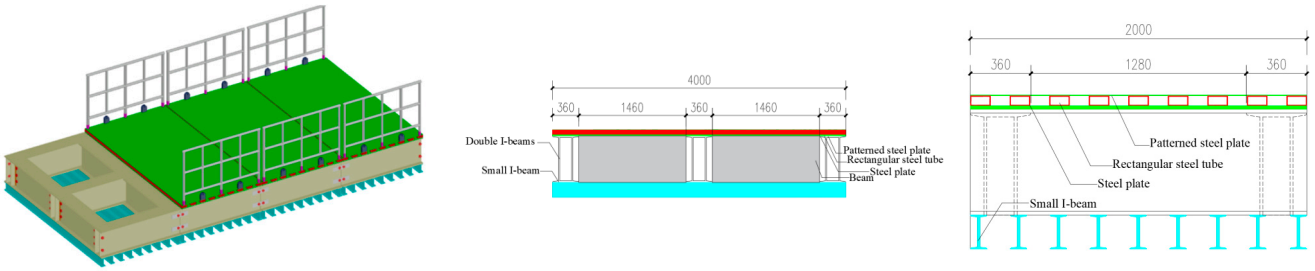
Embaby et al. [3] used a Bailey-beam type steel temporary bridge constructed from factory-processed "Type 321 prefabricated highway steel bridge" standard truss panels. The plates and sections were made of Q345B steel configured in a double-truss, single-layer bridge structure; however, such temporary bridges are excessively costly and bulky, making them unsuitable for complex or space-limited environments. Wang et al. [19] developed a novel adjustable steel module composed of a four-bar linkage capable of constructing efficient variable-depth arch bridges, yet the structure suffers from limited load-bearing capacity and complex on-site installation processes, restricting its practical application. Knight et al. [20] fabricated a prefabricated pedestrian footbridge using a folding technique in the Bracklinn Falls project, where the modular system effectively improved manufacturing efficiency by minimizing welding. Nonetheless, its load-bearing capacity is limited to pedestrian loads, failing to meet construction scenarios that demand the passage of heavy equipment.

This study aims to propose a generalized theoretical framework for analyzing modular composite steel temporary bridges deployed on soft foundation environments. First, an analytical model is established based on classic mechanics of materials and the theory of short elastic foundation beams. By incorporating the equivalent flexural stiffness of the composite cross-section, this model reveals that the mechanical response of the bridge on flexible soft foundations is dominated by rigid-body settlement. Then, a full-scale in situ static load test using a 25-ton crawler vehicle was conducted in a typical Northeast China paddy field to capture the overall settlement and local stress behavior of the novel composite temporary bridge under real soft-soil geological conditions. On this basis, a refined 3D numerical model was established via an FEA platform to validate the joint stress concentration effects induced by geometric discontinuities and the global anti-overturning stability under a 100-ton extreme heavy load and asymmetric eccentric loading conditions. The findings of this study not only show the collaborative load-bearing mechanisms of the plate–beam-soft foundation coupled system but also provide a scientific theoretical basis for the design and safety control of prefabricated temporary structures operating in extremely adverse geological conditions.

2. Structural Design and Theoretical Analysis

2.1. Structural Configuration Design

According to Chinese national standards, including the *Standard for Design of Steel Structures* (GB 50017-2017) [21], the *Specifications for Design of Highway Steel Bridges* (JTG D64-2015) [22], and the *Technical Standard for Prefabricated Steel Structure Buildings* (GB/T 51232-2016) [23], and tailored to the low bearing capacity and high deformability of soft paddy soil foundations, a novel portable steel bridge structure was designed, as illustrated in Figure 1.



(**a**) (**b**) (**c**)

Figure 1. Structural schematic of the portable steel bridge (mm). (**a**) Global numerical model; (**b**) Front view; (**c**) Side view of a single frame.

To ensure comprehensive structural safety, stability, and compatibility with the application environment, Q235 steel is selected for the primary load-bearing components. Parallel-welded double I-beams (Type 63c) serve as the primary longitudinal girders, connected via batten plates to form a composite cross-section that enhances both flexural and torsional rigidity. For the central longitudinal spans, 2 m specifications of the double I-beams are used, whereas 1.46 m specifications are deployed for side spans or transition segments requiring length adjustments. This combination allows for flexible adjustments of the bridge length.

Under the primary load-bearing beams, Type 20a I-beams are installed as the base structural frame to provide high flexural capacity and cost-effectiveness. A load-bearing interlayer consisting of a 20 mm steel plate and 120 × 60 × 5 mm rectangular steel tubes is positioned above the girders to distribute concentrated wheel loads and enhance structural integration. The driving surface is covered with a 4.5 mm non-slip checkered plate. All components are interconnected via welding with a minimum weld quality of Grade 2 to ensure rigid, stable, and highly integrated connections. Each modular frame measures 4 m in width and 2 m in length. Individual frames are interconnected longitudinally via high-strength bolts to form an integrated deck system, ensuring effective wheel load distribution and global stability.

2.2. Elastic Foundation Beam Theory for Temporary Bridges on Soft Foundations

To show the deformation behavior and load-transfer mechanisms of the novel prefabricated steel temporary bridge on extremely weak paddy foundations, the global structure is simplified into a Winkler elastic foundation beam model. Since the temporary bridge consists of multiple modules spliced transversely and connected continuously via longitudinal bolts, its mechanical behavior satisfies the fourth-order ordinary differential governing equation for a Winkler foundation beam:

$$EI_{\mathrm{eq}}\frac{d^4v(x)}{dx^4} + kbv(x) = q(x) \quad (1)$$

where $v(x)$ is the vertical deflection of the temporary bridge (m); $q(x)$ is the equivalent line load exerted by the upper construction machinery on the deck (kN/m); b is the total effective contact width between the modular bridge and the soft subgrade, taken as $b = 4$ m based on the design layout; k is the subgrade reaction coefficient (MN/m^3); EI_{eq} is the equivalent flexural rigidity of the cross-section of the upper steel temporary bridge (N·mm^2).

Based on the geometric configurations of the parallel double 63c I-beam main girders, 20a base I-beams, and the rectangular steel tube interlayer detailed in Section 2.1, the equivalent flexural rigidity of the prefabricated composite section was derived using the moment-area method and the stiffness equivalence principle: $EI_{eq} = 2.29 \times 10^{15}$ N·mm^2.

For the waterlogged, fluid–plastic muddy clay environment characteristic of Northeast China's summer paddy fields, and in accordance with the empirical constants stated in the *Specifications for Design of Foundation of Highway Bridges and Culverts* (JTG 3363-2019) [24] for soft-to-fluid–plastic cohesive soils, a conservative subgrade reaction coefficient characteristic value of $k = 15$ MN/m^3 (i.e., 1.5×10^4 kN/m^3) was selected for structural safety envelope design.

To characterize the relative stiffness ratio between the upper steel bridge structure and the underlying ultra-weak foundation, the core characteristic parameter $\lambda\left(\mathrm{m}^{-1}\right)$ of the Winkler foundation beam is introduced:

$$\lambda = \sqrt[4]{\frac{\mathrm{kb}}{4EI_{eq}}} \tag{2}$$

Substituting the geological parameters, design geometric dimensions, and equivalent flexural rigidity into Equation (2) yields a system characteristic parameter of $\lambda \approx 0.284$ m^{-1}. The total length of the temporary transit bridge developed in this study is $L = 8$ m, yielding a dimensionless structural stiffness characteristic value of: $\lambda L = 0.284 \times 8 = 2.272$.

According to the theory of finite-length elastic foundation beams, when the stiffness characteristic value satisfies $\lambda L < \pi$, the mechanical behavior of the structure can be classified as a classic short beam (or rigid beam). This criterion demonstrates that under heavy machinery loads, the steel superstructure will not undergo significant localized flexible bending. This rigid beam characteristic allows concentrated mid-span loads to diffuse uniformly and rapidly into the foundation through the high-rigidity double main beams and spatial interlayer, significantly reducing the local bending stress reserve within the main girders.

The establishment of this mechanical mechanism theoretically clarifies the safe operational mode of the structure on extreme soft foundations. It also explains the exceptionally low local bending stresses observed in the bridge deck plates during subsequent in situ static load tests, while providing a core mechanical baseline for the non-linear elastic–plastic foundation-structure 3D finite element model established later in this study.

3. In Situ Static Load Testing

3.1. Experimental Program

To evaluate the structural response, stress distribution, and foundation adaptability of the temporary bridge under a 25-ton load, a large-scale in situ static load test was conducted in a typical agricultural paddy field region in Northeast China, as shown in Figure 2. Prior to the static load testing, a site-specific geotechnical investigation was conducted to determine the foundation parameters. This investigation comprised Portable Vane Shear Tests, Dynamic Cone Penetration Tests, and laboratory analysis of undisturbed soil samples. The tests identified a two-layer stratified soil profile typical of the region: a 0.5-m-thick

upper layer of saturated, fluid–plastic silty clay (paddy mud) exhibiting extremely low bearing capacity, underlain by a significantly stiffer and denser silty clay layer.

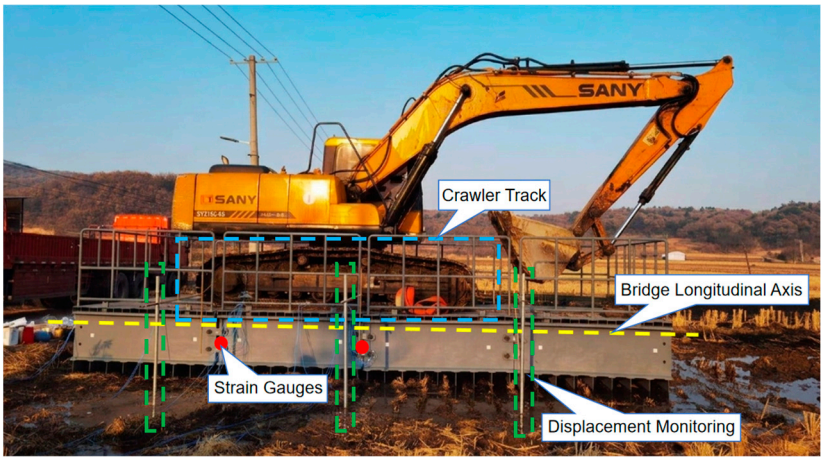


Figure 2. Field setup for the in situ static load test.

The experimental bridge had a total length of 8 m and was composed of four standardized modules measuring 4 m in width and 2 m in length. Main girders of adjacent modules were securely fastened via high-strength bolts and steel splice plates. A typical crawler construction vehicle with a gross weight of 25 tons served as the static load source. The vehicle was guided slowly to the longitudinal and transverse geometric center of the temporary bridge and parked. Component strains and bridge settlements were recorded to assess the maximum bending stress and maximum vertical deflection of the structure. Five electrical resistance strain gauges were installed across the bridge deck, side-span transverse beams, and connection splice plates, as illustrated in Figure 3.

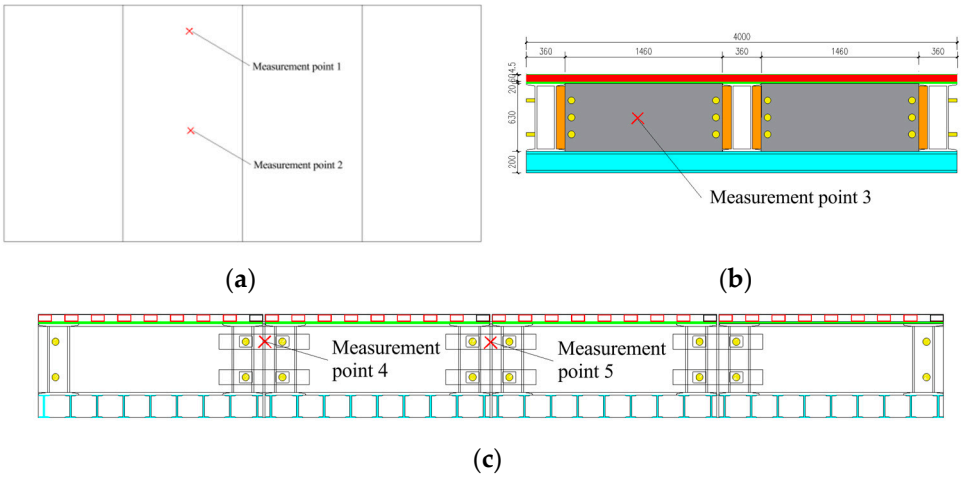


Figure 3. Layout of instrumentation points. (**a**) Measurement points on the bridge deck; (**b**) Measurement point on the transverse beam; (**c**) Measurement points on the splice plate.

In addition to the strain gauges, macroscopic displacement monitoring devices were arranged around the field test site to continuously record the global vertical settlement of the temporary bridge under loading.

3.2. Test Results and Discussion

After the 25-ton heavy crawler construction vehicle was brought to a stop at the geometric center of the bridge, the strains at each measurement point were collected once

the structural mechanical response stabilized. The converted stress results are summarized in Table 1.

Table 1. Converted stress results under the 25-ton loading condition.

Measurement Point	Deck Plate 1	Deck Plate 2	Transverse Beam 3	Splice Plate 4	Splice Plate 5
Converted Stress (MPa)	2.2	0.9	0.3	18.5	63.7

The in situ test results indicate that the structural components of the temporary bridge system maintained an excellent load-bearing state under the 25-ton crawler vehicle load. The converted stresses at deck plate points 1 and 2 were 2.2 MPa and 0.9 MPa, respectively, while the stress at transverse beam point 3 was only 0.3 MPa. This indicates that the deck system—composed of the 4.5 mm checkered plate, 20 mm load-bearing steel plate, and 120 × 60 × 5 mm rectangular steel tube interlayer—possesses exceptionally high local mid-span flexural rigidity and spatial collaborative load-transfer capability. The localized heavy load from the vehicle crawlers was rapidly and uniformly dispersed to the underlying double 63c main longitudinal girders and the broader beam system through the highly rigid deck interlayer, keeping local bending stresses in the deck plate at a negligible level.

The maximum stress within the system occurred at the longitudinal high-strength bolted steel splice plates between the modular segments, where the stress at point 4 reached 18.5 MPa, and point 5 registered the peak value of 63.7 MPa. Because the temporary bridge is a simply supported system longitudinally assembled from four 2 m modules via high-strength bolts, the global structure experiences its maximum positive bending moment when the vehicle is positioned at the geometric center (mid-span). Consequently, the splice plates, serving as the core shear and tensile load-transfer components across the splicing interface, must bear the longitudinal tensile stresses arising from global bending as well as inter-module shear transfer. Compared with the continuous cross-section of the main girders, the spliced interface presents distinct geometric and stiffness discontinuities, thereby generating obvious stress concentrations that caused the stress at point 5 to be significantly higher than those in the deck plates and transverse beams.

Despite the elevated stress state at the splice plate due to stress concentrations, the peak value remains far below the design yield strength of 235 MPa for Q235 steel. The entire structure operated well within the linear elastic range, demonstrating a sufficient safety margin for load capacity. Furthermore, during the static parking of the 25-ton heavy vehicle, the 20a I-beam bases at the bottom of the temporary bridge effectively expanded the bearing contact area; no obvious differential settlement or sudden catastrophic overturning instability was observed during the field test.

4. Finite Element Modeling and Parameter Analysis

4.1. Model Development

A refined 3D numerical analysis model of the novel prefabricated steel temporary bridge was established using the finite element software Abaqus (2021). The bridge model has a total length of 8 m and comprises four 2 m long, 4 m wide standardized modules. Q235 steel properties were applied to the entire bridge structure, and the summer paddy soil was modeled with stratified layers based on field conditions: a 50 cm upper soft soil layer and an underlying hard soil layer. The elastic–plastic behavior of both soil layers was simulated using the Mohr-Coulomb plasticity model, which is widely adopted and well-suited for capturing the shear failure and yielding characteristics of continuous foundations under heavy loads. The material parameters are detailed in Tables 2 and 3.

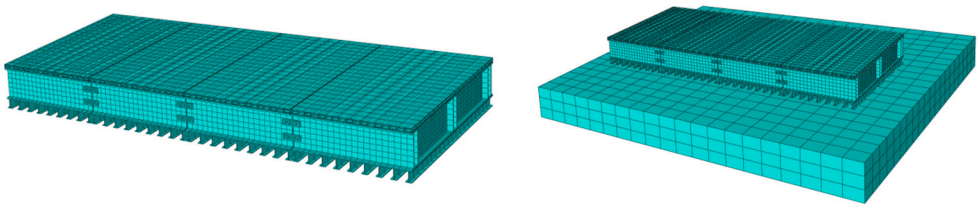
Table 2. Material parameters for Q235 steel.

Material	Density (g/cm^3)	Elastic Modulus (GPa)	Poisson's Ratio	Yield Strength (MPa)
Q235 Steel	7.85	210	0.3	235

Table 3. Geotechnical parameters for the stratified soil foundation.

Material	Density (g/cm^3)	Elastic Modulus (MPa)	Poisson's Ratio	Friction Angle	Dilation Angle	Cohesion Yield Stress (kPa)
Soft Soil	1.8	10	0.3	32°	5°	15
Hard Soil	2	100	0.3	32°	5°	50

To balance computational accuracy and efficiency given the structural complexity, a partitioned meshing strategy was implemented (Figure 4). Three-dimensional solid components—including the double 63c main longitudinal I-beams, 20a base I-beams, and the rectangular steel tube interlayer—were modeled using 8-node linear brick, reduced-integration elements (C3D8R). The mesh size for the primary load-bearing members was maintained between 100 mm and 200 mm, while local mesh refinement was applied at stress-concentration zones such as bolt holes and core longitudinal-transverse beam intersections, where the mesh size was refined to 20 mm. The results indicated that once the element size at the critical stress zones (such as the splice plates and load-bearing contact areas) was refined to 20 mm, the variation in the peak Mises stress stabilized at less than 2%, ensuring excellent numerical accuracy without excessive computational cost. For completeness of the numerical model description, the final meshed model of the coupled bridge–foundation system comprised a total of 141,700 elements and 71,377 nodes.



(**a**) (**b**)

Figure 4. Finite element mesh generation. (**a**) Temporary bridge mesh; (**b**) Foundation soil mesh.

To eliminate artificial edge effects and ensure a realistic representation of the semi-infinite foundation, the computational soil domain was deliberately extended. While the temporary bridge measures 8 m × 4 m, the soil block was modeled with dimensions of 24 m (Length) × 12 m (Width) × 10 m (Depth), extending 8 m longitudinally and 4 m transversely from the bridge edges. The 10 m depth comprises the 0.5 m soft soil layer and a 9.5 m stiff underlying layer. Regarding the boundary conditions of the soil domain, the bottom surface was completely fixed against translation in all spatial directions ($U_1 = U_2 = U_3 = 0$) to simulate a semi-infinite foundation and eliminate stress wave reflection, while the four lateral boundaries were constrained normally to their respective planes. For the interaction interfaces, a surface-to-surface contact algorithm was employed. The normal behavior was defined as 'Hard Contact' to prevent non-physical penetration between the steel base and the soft soil, while the tangential behavior utilized the Penalty friction formulation. Furthermore, Tie constraints were utilized to simulate the bolted joints between modular units. This simplification is theoretically justified because the primary objective of this continuum model is to capture the macroscopic global rigid-body settlement and the primary stress distribution of the main girders, rather than the localized micro-slip mechanics of

individual bolt threads. Utilizing Tie constraints successfully maintains the global stiffness equivalence while significantly preventing local non-convergence issues.

It should be noted that while the analytical framework in Section 2.2 adopts a classic Winkler foundation simplification to qualitatively determine the bridge's operating category (i.e., a rigid short beam), the numerical model transitions to a 3D continuum discretization approach. The continuous formulation using solid soil elements overcomes the Winkler limitation of neglected shear interaction between soil columns. The input elastic modulus (E = 10 MPa) for the 0.5-m-thick soft layer closely aligns with the vertical stiffness boundary (k = 15 MN/m^3) used in the analytical safety envelope design, according to one-dimensional compression mechanics (Equation (3)). This progression from an analytical baseline to an elastic–plastic continuum simulation ensures both macroscopic structural classification and localized quantitative accuracy.

$$k \approx \frac{E}{H(1-\nu^2)} \tag{3}$$

To accurately represent traffic loads without inducing non-physical stress concentrations, all vehicle loading configurations were modeled as uniform surface pressures applied over idealized contact patches. For crawler cases, the load was distributed across two parallel rectangular strips (3.6 m × 0.6 m each, spaced 2.4 m apart), yielding a surface pressure of 57.87 kPa per track under the 25-ton standard case. For the six-wheel truck, the load was discretized into six rectangular wheel prints (0.2 m × 0.3 m each) with axle loads partitioned in a 1:2 ratio between the front and rear tandem axles, ensuring consistency with empirical wheel pressure distributions.

Using this validated 3D finite element model, the static responses of the novel prefabricated temporary steel bridge under various construction vehicle configurations were comprehensively evaluated. The numerical simulation included six representative load cases representing crawler-type and six-wheel construction machinery under a 25-ton standard load, a 100-ton extreme load, and eccentric loading conditions (Figures 5 and 6, Table 4).

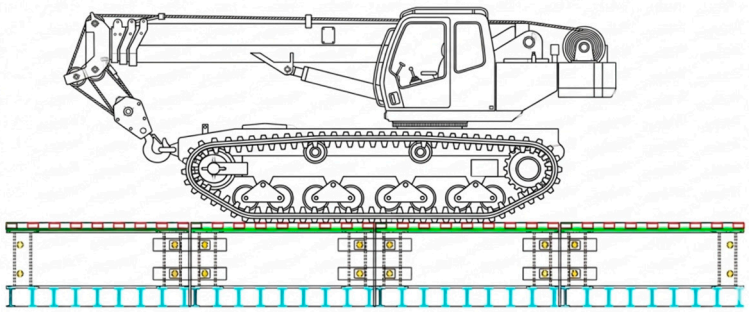


Figure 5. Schematic of the static load layout for the crawler vehicle.

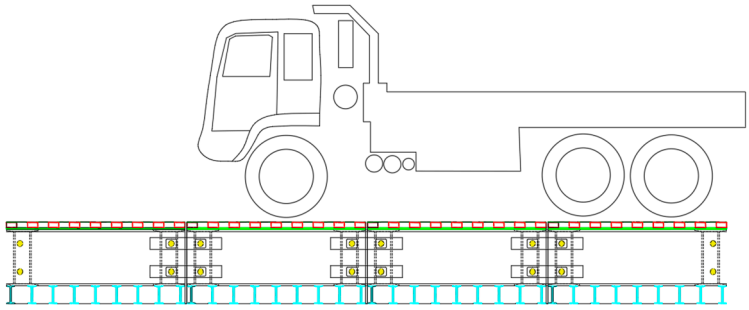


Figure 6. Schematic of the static load layout for the six-wheel truck.

Table 4. Matrix of simulated loading cases.

Load Case	Vehicle Type	Gross Weight (t)	Load Configuration
Case 1	Crawler Vehicle	25	Centered at mid-span
Case 2	Crawler Vehicle	100	Centered at mid-span
Case 3	Six-wheel Truck	25	Centered at mid-span
Case 4	Six-wheel Truck	100	Centered at mid-span
Case 5	Crawler Vehicle	35	Eccentric layout (20 t on one side, 15 t on the other)
Case 6	Crawler Vehicle	25	During the process of getting on the bridge

4.2. Validation of the Finite Element Model

To verify the accuracy of the numerical simulation, the empirical data from the 25-ton crawler vehicle mid-span static load test were compared against the finite element calculation results. As shown in Table 5 and Figure 7, the numerical model captured the spatial stress distribution across components with high accuracy. Under heavy loads, the deck system exhibited superior collaborative behavior, maintaining stresses in the deck plate and transverse beams below 3 MPa.

Table 5. Comparison between experimental measurements and numerical predictions.

Measurement Point	Deck Plate 1	Deck Plate 2	Transverse Beam 3	Splice Plate 4	Splice Plate 5
Experimental Stress (MPa)	2.2	0.9	0.3	18.5	63.7
Simulated Mises Stress (MPa)	1.81	0.83	0.19	17.75	61.20
Relative Error	17%	7%	36%	4%	3.92%

Due to the stiffness discontinuity at the longitudinal inter-module joints, an obvious stress concentration was confirmed at the mid-span splice plates. The empirical peak stress at this location was 63.7 MPa, compared to the numerical prediction of 61.20 MPa, yielding a relative error of only 3.92% for point 5. The simulated stresses at key points were slightly higher or lower than the measured data due to the idealized rigid simplification of the bolted interfaces and the ignored elastic–plastic damping effects of the actual paddy subgrade. Overall, the relative errors at critical locations remained strictly within acceptable engineering limits, validating the element selection, mesh densities, and boundary condition definitions.

Beyond the localized stress validation at the five representative points, the spatial deflected shape and soil-structure interaction of the FE model were rigorously verified using the macroscopic settlement data. Field measurements from the surrounding displacement monitoring devices indicated that the temporary bridge primarily underwent a global rigid-body settlement, with an actual recorded maximum vertical displacement of 1.52 mm under the 25-ton load. The FEA model accurately replicated this settlement pattern, predicting a peak displacement of 1.41 mm. The relative error in macroscopic settlement between the numerical simulation and the in situ measurement was merely 7.2%. This close agreement in both local stress distribution and global spatial kinematics confirms that the numerical model is highly reliable.

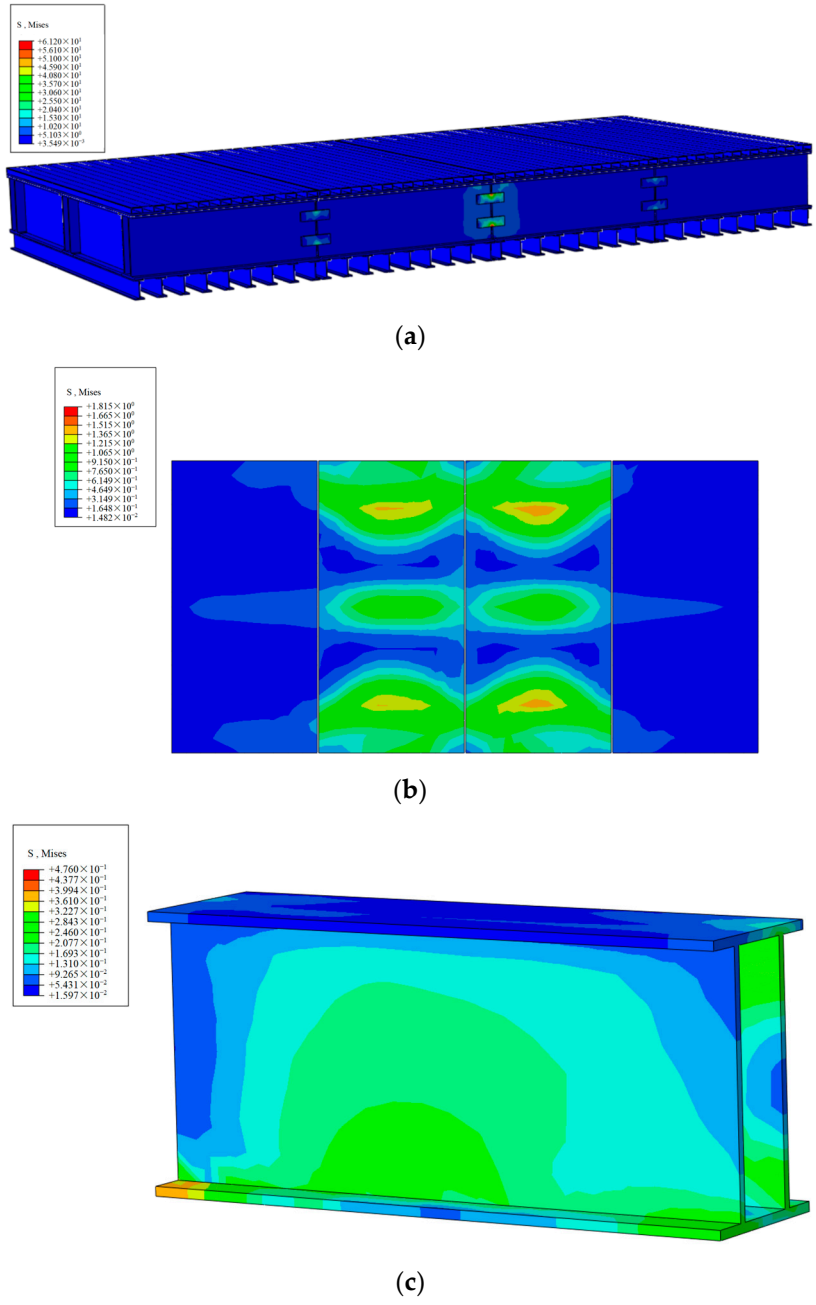


Figure 7. Mises stress contours for Load Case 1. (**a**) Global structure; (**b**) Bridge deck plate; (**c**) Transverse beam.

4.3. Parametric Analysis of Mechanical Behavior Under Multiple Load Cases

The simulated stress and displacement contours for the remaining five load cases are displayed in Figures 8–14. Under standard 25-ton construction vehicle loads, the temporary bridge operated entirely within the linear elastic range. In Load Case 1 (Figure 7), the maximum Mises stress was concentrated at the inter-module high-strength bolted splice plates, peaking at 61.2 MPa. Stress distributions across primary members—such as the deck plates, rectangular tube interlayers, and main transverse beams—were highly uniform and low, with peak values of only 3.742 MPa. For the 25-ton six-wheel truck load case (Case 3, Figure 10), despite the higher concentration of wheel contact pressures, the high stiffness of the main girder system limited the maximum splice plate stress to 45.06 MPa and the deck plate stress to 2.933 MPa. Furthermore, simulation of the 25-ton crawler vehicle entering the bridge end (Case 6, Figure 14) demonstrated a smooth stress transition

into the longitudinal structure, yielding a peak splice plate stress of only 19.37 MPa without sudden stress concentrations.

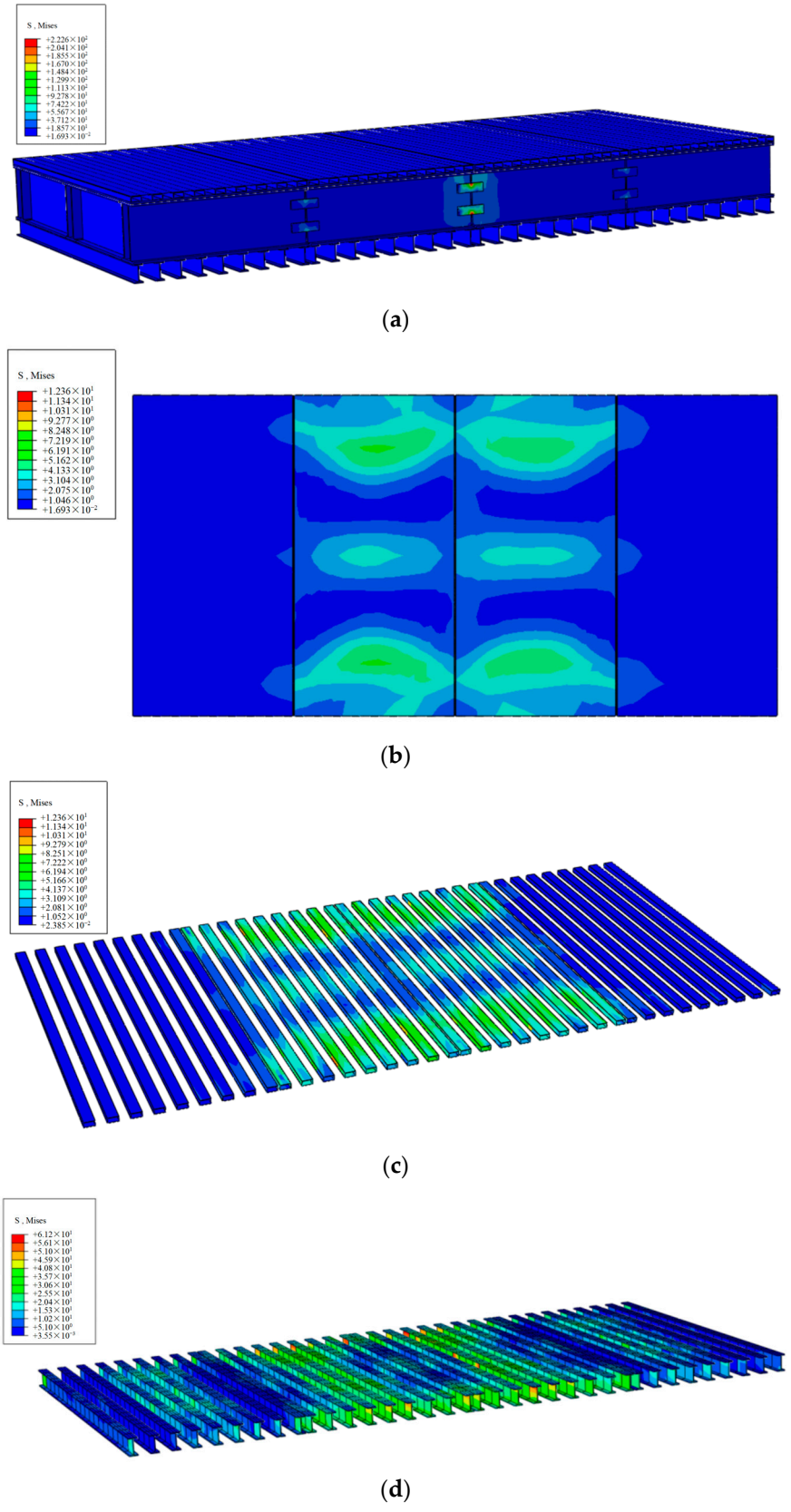


Figure 8. Mises stress contours for Load Case 2. (**a**) Global structure; (**b**) Bridge deck plate; (**c**) Rectangular steel tube interlayer; (**d**) I-beam base frame.

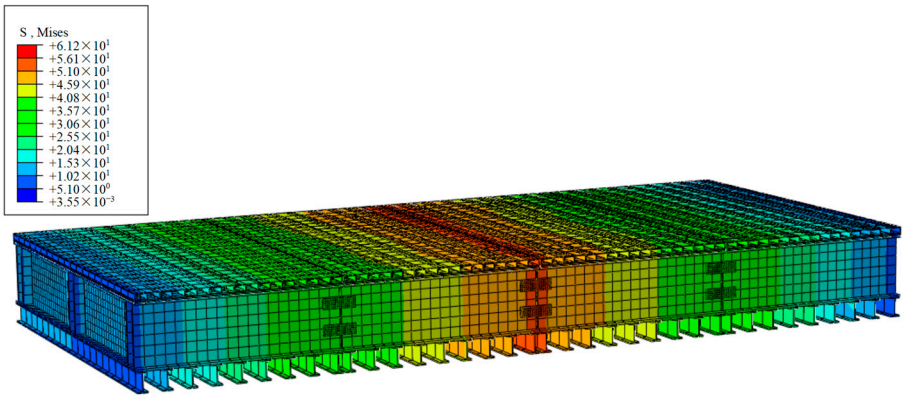
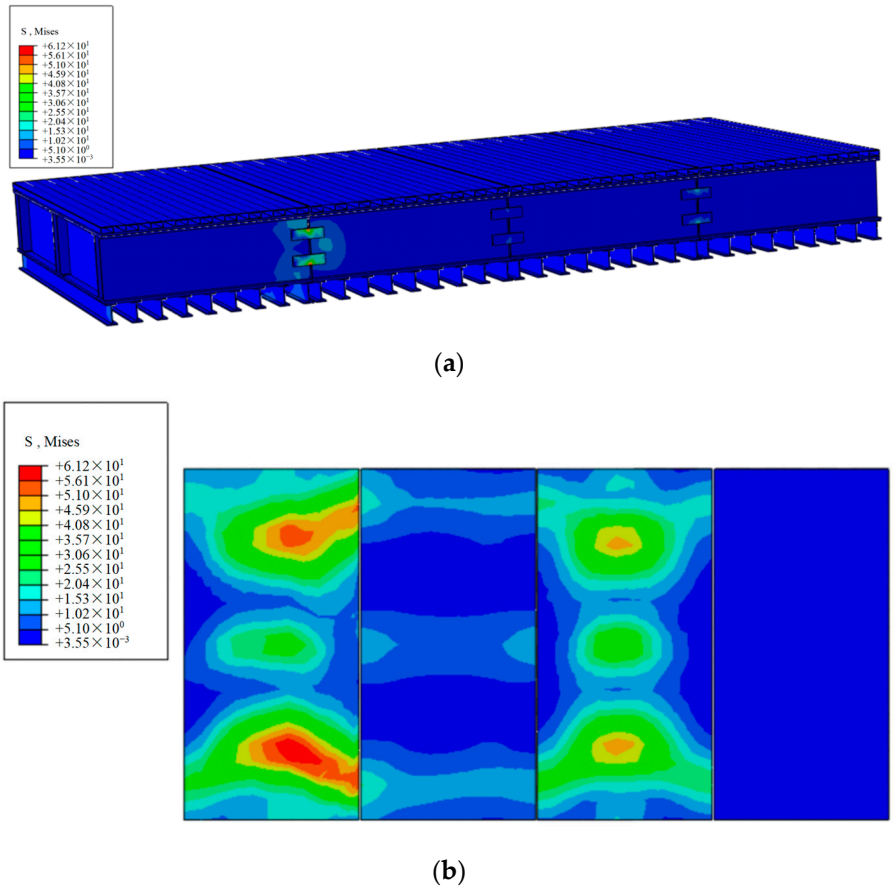


Figure 9. Displacement contours for Load Case 2.



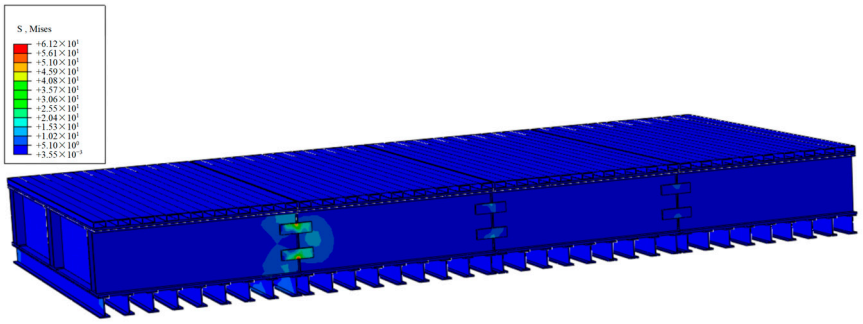
(**a**)

(**b**)

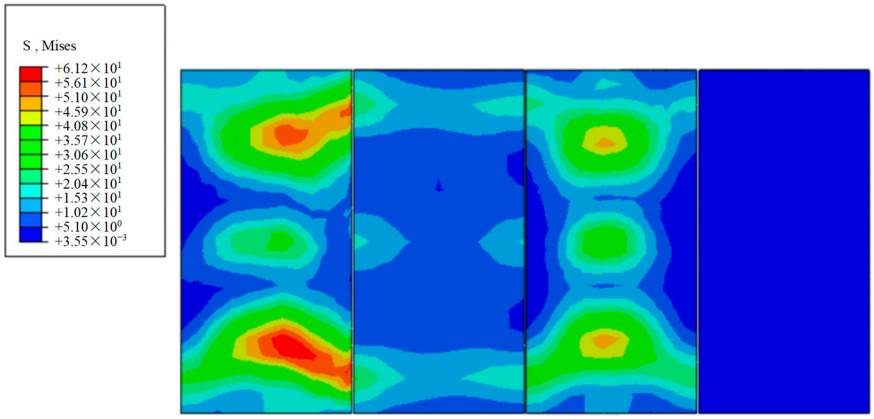
Figure 10. Mises stress contours for Load Case 3. (**a**) Global structure; (**b**) Bridge deck plate.

To quantify the ultimate safety margins of the temporary bridge under extreme field scenarios, its structural resistance against a 100-ton extreme load was investigated. As illustrated in the stress contours of Figure 8, the structural components successfully redistributed the massive load. The global bending moment primarily localized the maximum stress at the inter-module splice plates (Figure 8a), which reached 222.6 MPa. While this value approaches the 235 MPa yield strength limit of Q235 steel, the deck plates (Figure 8b), the rectangular steel tube interlayer (Figure 8c), and the base frames (Figure 8d) remained at low stress levels (below 4 MPa). This indicates that the system preserves a functional safety margin and effectively prevents localized material yielding. Furthermore, the displacement contour presented in Figure 9 reveals that the peak vertical displacement extracted at mid-span was 5.624 mm. This visual distribution of settlement confirms that the rigid-body sinking mechanism dominates on the soft foundation, strictly satisfying the deflection

limit of L/500 (i.e., 8 mm) specified in the *Specifications for Design of Highway Steel Bridge* (JTG D64-2015).



(**a**)



(**b**)

Figure 11. Mises stress contours for Load Case 4. (**a**) Global structure; (**b**) Bridge deck plate.

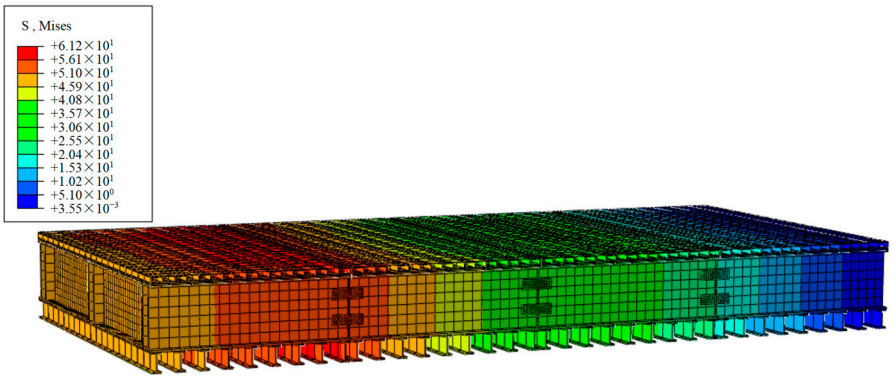


Figure 12. Displacement contours for Load Case 4.

It must be clarified that the 100-ton extreme load is investigated not as a routine operational condition, but as an Accidental or Ultimate Limit State scenario. In actual summer power line construction in paddy fields, while 25-ton to 35-ton machinery constitutes the routine traffic, the emergency deployment of heavier equipment, compounded by dynamic impact factors, can temporarily subject the bridge to significantly higher equivalent static loads. Although the peak localized stress of 222.6 MPa at the splice plates approaches the 235 MPa yield strength of Q235 steel under this extreme load, the primary main girders remain safely within a low-stress elastic range. This demonstrates a robust global safety factor of approximately 4.0 relative to the 25-ton design load. Considering the temporary nature of the structure, strictly controlled traffic speeds, and the excellent ductility of Q235 steel,

this localized stress reserve is theoretically acceptable. It scientifically ensures that the modular bridge will not suffer catastrophic global collapse under unforeseen heavy traffic.

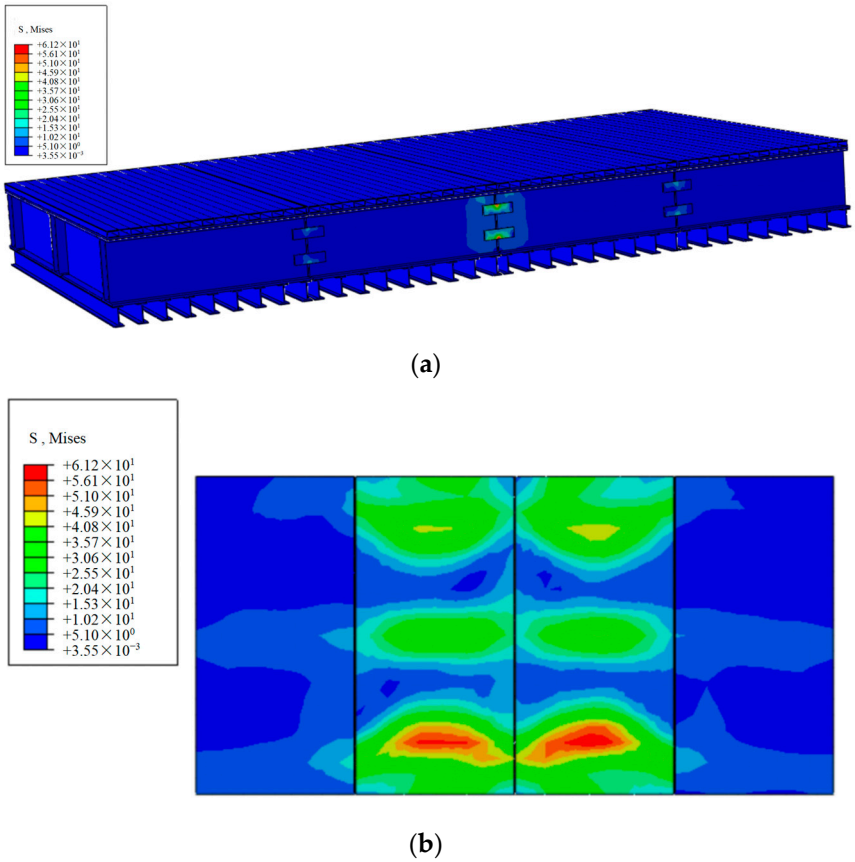


Figure 13. Mises stress contours for Load Case 5. (**a**) Global structure; (**b**) Bridge deck plate.

Compared to crawler vehicles, six-wheel trucks exert highly concentrated wheel contact pressures on the driving surface. The stress distribution for the 25-ton six-wheel truck load case (Case 3) is presented in Figure 10. Despite the severe concentration of localized wheel loads, the global structure (Figure 10a) exhibits a maximum splice plate stress of only 45.06 MPa. More importantly, the localized stress contour of the deck plate (Figure 10b) demonstrates that the rectangular steel tube interlayer efficiently diffuses the concentrated wheel footprint forces into the underlying main girders. Consequently, the peak bending stress in the deck plate is limited to a negligible 2.933 MPa, proving the exceptional local flexural rigidity of the designed composite deck system.

Under an identical 100-ton extreme load delivered by the six-wheel truck (Case 4), the structural response is captured in Figures 11 and 12. The maximum Mises stress (Figure 11a) reached 160.4 MPa at the mid-span longitudinal joints. The footprint stress patterns are distinctly visible on the deck plate (Figure 11b), yet the local stress remains safely below the yield threshold. Simultaneously, the vertical displacement contour (Figure 12) shows a maximum deflection of 4.749 mm. These results confirm that the prefabricated deck system offers high flexural rigidity and additional safety margins for heavy equipment transits.

To simulate crane lifting operations common in power line construction, an asymmetric eccentric load case representing a 35-ton equipment configuration was evaluated (Case 5, Figure 13). Under obvious asymmetric loading, the deck plates experienced eccentric compression and a minor twisting tendency (Figure 13b). Following stress redistribution, the peak stress remained confined to the splice plate region at 105.2 MPa (Figure 13a), while the maximum stress in the load-bearing deck plate was limited to 2.608 MPa. The interfaces

between the base I-beams and the underlying soft clay sustained stable contact bonding, and the global structure exhibited neither material yield failure nor overturning instability.

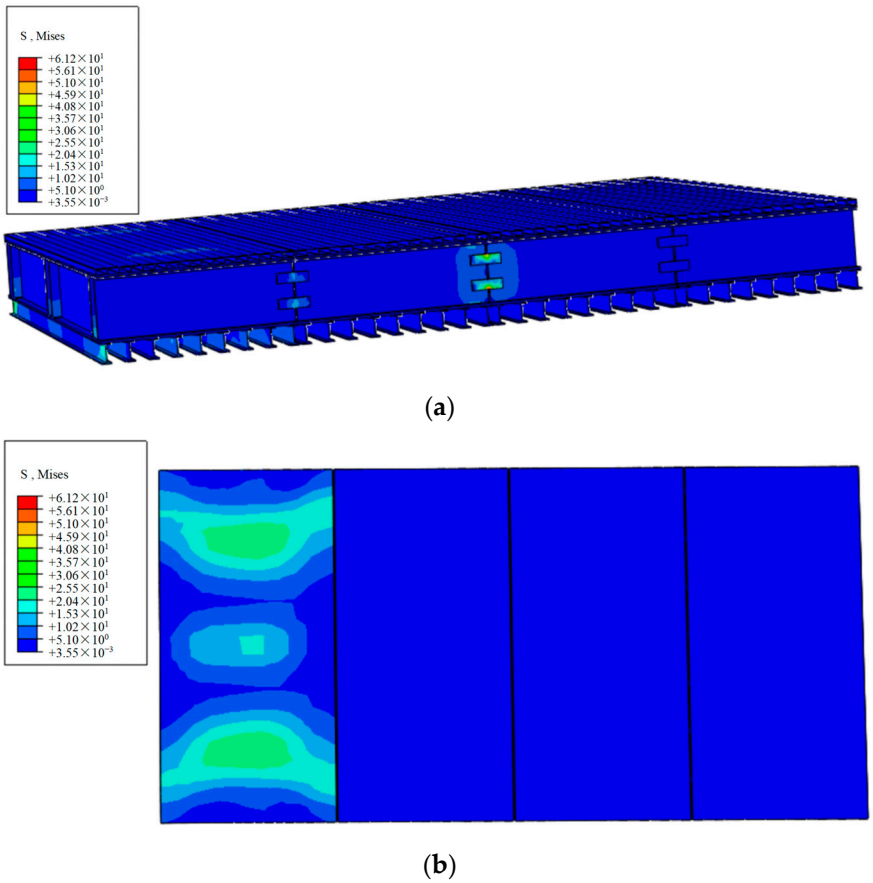


Figure 14. Mises stress contours for Load Case 6. (**a**) Global structure; (**b**) Bridge deck plate.

Finally, Figure 14 illustrates the structural behavior during the critical transient phase when a 25-ton crawler vehicle enters the bridge end (Case 6). The stress contour of the global structure (Figure 14a) and the deck plate (Figure 14b) demonstrates a smooth stress transition from the soil foundation into the longitudinal steel structure. The peak splice plate stress is recorded at only 19.37 MPa, indicating the absence of sudden stress concentrations or catastrophic local buckling at the support boundary. This verifies that the temporary bridge system maintains excellent structural safety during the initial load-transfer phase as heavy machinery mounts the deck.

In summary, the structural strength, stiffness, and anti-overturning stability of the proposed prefabricated modular temporary bridge meet all design benchmarks, providing a secure and reliable temporary transit solution for heavy power grid construction machinery operating on weak paddy field foundations.

4.4. Sensitivity Analysis of Foundation Parameters

To systematically evaluate the structural adaptability and reliability of the temporary bridge across highly variable agricultural environments, a parametric sensitivity analysis was conducted. In paddy fields, the geotechnical properties of the upper silty clay fluctuate significantly with moisture content. Therefore, the elastic modulus and cohesion yield stress of the soft layer were varied simultaneously to represent realistic physical soil states. The parameters ranged from an extreme fluid–plastic state (E = 5 MPa, c = 10 kPa) to a partially consolidated state (E = 20 MPa, c = 20 kPa). All simulations were executed under the 100-ton extreme mid-span crawler loading (Case 2) to establish a rigorous safety envelope.

The macroscopic deformation of the coupled system is highly sensitive to foundation stiffness. As summarized in Table 6, at the extreme lower bound (E = 5 MPa), the maximum mid-span vertical settlement escalates to 9.82 mm, a 74.6% increase relative to the baseline condition. Conversely, strengthening the subgrade to a partially consolidated state (E = 20 MPa) suppresses the maximum vertical deformation to 3.15 mm. This pronounced variation highlights the critical role of the base I-beam frames in adapting to severe subgrade deformations and preventing localized punching failures within the ultra-weak soil.

Table 6. Structural response parameters under varying soft soil conditions (100-ton extreme load).

Soil State	Elastic Modulus (MPa)	Cohesion Yield Stress (kPa)	Max Mid-Span Settlement (mm)	Peak Mises Stress at Splice Plates (MPa)
Extreme fluid–plastic	5	10	9.82	226.8
Baseline	10	15	5.62	222.6
Partially consolidated	20	20	3.15	215.3

In stark contrast to the settlement sensitivity, the internal stress fields of the steel superstructure maintain exceptional stability against foundation variations. As the soil softens, the peak Mises stress localized at the critical splice plates experiences minimal variation, fluctuating within a narrow band of 215.3 MPa to 226.8 MPa (approximately a 5% deviation). This stress insensitivity validates the theoretical deduction in Section 2.2: the modular bridge operates strictly within a classic "rigid short beam" regime. Foundation softening induces a global rigid-body sinking mechanism rather than severe localized bending. Consequently, the temporary bridge maintains dependable load-bearing capacity without structural yielding, confirming its applicability on extremely weak foundations.

4.5. Comparative Discussion and Structural Novelty

To explicitly quantify the structural novelty and practical advantages of the proposed system, a comprehensive comparison with classic Bailey bridges and traditional temporary subgrade treatments (e.g., gravel replacement with steel plates) is summarized in Table 7.

Currently, no specific modular bridge exists that is specifically tailored for short-term, rapid assembly directly on untreated fluid–plastic paddy fields. Traditional Bailey bridges, while highly versatile, are inherently designed as large, expensive permanent or semi-permanent structures for longer spans. They rely predominantly on global truss action to resist bending and strictly require stable, highly compacted concrete or timber abutments to prevent catastrophic differential settlement. Consequently, their primary deformation mode under load is structural flexure.

In stark contrast, the proposed modular bridge is distinctively engineered for immediate placement on continuous, ultra-weak mud without the need for costly and time-consuming ground treatments. As verified by the in situ measurements (Section 4.2) and numerical simulations (Section 4.3), the structure operates on a fundamentally different mechanical principle: the "rigid short beam" mechanism. Instead of experiencing significant global bending, the heavy vehicle loads (up to 100 tons) are effectively planarized by the continuous I-beam base frames, resulting in a controlled, uniform rigid-body settlement (a maximum measured deflection of merely 1.52 mm under a 25-ton load).

Furthermore, from a construction management perspective, the proposed system drastically reduces material consumption and assembly time. For a typical 8 m span, the proposed bridge can be assembled by a standard crane in approximately 2 h, whereas a comparable Bailey bridge or deep gravel stabilization would require multiple days of heavy earthwork and site preparation. By circumventing the need for deep foundation

stabilization and minimizing structural weight, the proposed system offers a uniquely cost-effective, environmentally low-impact, and highly reliable solution specifically optimized for summer power line construction.

Table 7. Quantitative comparison of temporary access solutions for soft paddy fields (based on an 8 m-span requirement).

Evaluation Metric	Proposed Modular Steel Bridge	Classic Bailey Bridge (e.g., CB100)	Traditional Method (Gravel + Steel Plates)
Foundation Requirement	Direct placement on untreated soft mud	Requires firm, compacted abutments	Requires deep soil excavation and replacement
Primary Deformation Mode	Uniform rigid-body settlement	Global flexural bending	Local punching shear/Subgrade yielding
Assembly Time	~2 h (Rapid mechanical splicing)	1 to 2 days (Manual/mechanical assembly)	3 to 5 days (Extensive earthwork)
Material Consumption	~12 tons of steel (Optimized deck and base frames)	~16 tons of steel (Heavy trusses and transoms for heavy-duty limits)	~50 m^3 of gravel + ~10 tons of steel plates
Reusability	100% (Fully demountable)	100%	Low (Gravel is unrecoverable)
Overall Cost	~120,000 RMB (Cost-effective)	~160,000 RMB (High material and assembly cost)	~180,000 RMB (High earthwork and ecological recovery cost)

5. Conclusions

To address engineering challenges involving the low bearing capacity of soft paddy foundations in Northeast China and the resulting traffic constraints during summer power line construction, a modular prefabricated steel temporary bridge system was developed. Based on theoretical derivations, field testing, and numerical simulations exploring its mechanical response and structural safety, the following main conclusions are drawn:

(1) Theoretical analysis based on the Winkler elastic foundation beam model demonstrates that the dimensionless structural stiffness parameter is sufficiently small ($\lambda L < \pi$). When subjected to load, the global stiffness of the bridge structure is significantly higher than that of the underlying soil foundation. Consequently, the bridge responds primarily via uniform rigid-body settlement rather than severe localized flexible bending, effectively reducing the risks associated with differential settlement on weak subgrades.

(2) Under a standard 25-ton construction machinery load, the maximum Mises stress and vertical deflection at mid-span remain far below the material yield limits and design code thresholds. The structural components exhibit excellent collaborative performance, fully satisfying transit safety requirements for summer power line construction.

(3) Under extreme loading scenarios—including a 100-ton heavy crawler vehicle load and asymmetric eccentric loads—the maximum Mises stress at the main longitudinal girders and splice plates reached 222.6 MPa, approaching the yield strength limit of Q235 steel and indicating a full-load operational state. Finite element simulations highlight that the semi-rigid characteristics and localized stress concentration effects at the high-strength bolted inter-module joints represent critical factors governing the safety of temporary structures.

(4) The integrated "theoretical-experimental-numerical" analysis approach presented in this study successfully quantifies the non-linear evolution of discontinuous assembly interfaces within a structural-soft foundation system, serving as a valuable reference for the design of temporary structures on similar soft ground.

Finally, it is important to acknowledge the limitations of the current study. The experimental and numerical validations were conducted based on a specific modular geometry, Q235 steel grade, and the distinct stratified soft-soil profile of Northeast China's summer paddy fields under static loading conditions. Notably, the in situ field validation was restricted to a single loading position (mid-span) and a specific magnitude (25 tons), which may not fully encapsulate the structural response under varied eccentric or dynamic moving loads. Additionally, while the finite element simulation effectively captured the global rigid-body behavior, it utilized idealized rigid connections for simplicity, whereas actual field conditions involve loose bolt holes that could introduce minor localized slips. The extrapolation of these findings to entirely different geotechnical environments requires further site-specific verification. Furthermore, this study focuses purely on the static and pseudo-static structural responses. Future research should investigate the dynamic vehicle–bridge interaction, the long-term settlement under cyclic loading, and the fatigue assessment of the bolted splice joints under repeated heavy construction traffic.

Author Contributions: Conceptualization, D.S. and Z.C. (Zhaoqing Chen); methodology, D.S. and Z.C. (Zhaoqing Chen); investigation, D.S.; resources, Y.B.; data curation, Z.C. (Zhongzheng Cui) and Z.K.; writing—original draft preparation, D.S.; writing—review and editing, Z.C. (Zhongzheng Cui) and D.H.; supervision, D.H. and Y.B.; funding acquisition, Z.C. (Zhaoqing Chen) and D.H. All authors have read and agreed to the published version of the manuscript.

Funding: This research was funded by "Research and Application of Prefabricated Modular Temporary Bridges for Summer Power Line Construction on Northeast Paddy Field Soft Foundations" from State Grid Jilin Electric Power Co., Ltd. (2025-09).

Data Availability Statement: The original contributions presented in this study are included in this article. Further inquiries can be directed to the corresponding author.

Conflicts of Interest: Author Dongrui Song, Dong Han, Yanyang Bai and Zhongfeng Kan were employed by State Grid Jilin Electric Power Co., Ltd. The remaining authors declare that this research was conducted in the absence of any commercial or financial relationships that could be construed as potential conflicts of interest.

References

1. Khan, M.A. *Accelerated Bridge Construction: Best Practices and Techniques*; Butterworth-Heinemann: Oxford, UK, 2014.
2. Gerbo, E.J.; Casias, C.M.; Thrall, A.P.; Zoli, T.P. New bridge forms composed of modular bridge panels. *J. Bridge Eng.* **2016**, *21*, 04015084. [CrossRef]
3. Embaby, M.; El Naggar, M.H. Experimental and analytical investigation for modular double truss bridge. *Eng. Struct.* **2025**, *322*, 119087. [CrossRef]
4. Embaby, M.; El Naggar, M.H. Experimental and numerical investigation for steel shear panels of modular bridge. *J. Constr. Steel Res.* **2024**, *219*, 108743. [CrossRef]
5. Luo, L.; Li, Y.; Dai, H.; Sun, H.; Jia, M.; Yuan, H.; Cheng, X. Seismic performance prediction and interpretation of RC bridges under vehicle-bridge interaction: From VBI system simulation to ensemble learning surrogate models. *Eng. Struct.* **2025**, *341*, 120816. [CrossRef]
6. Bao, A.; Guillaume, C.; Satter, C.; Moraes, A.; Williams, P.; Kelly, T.; Guo, Y. Testing and evaluation of web bearing capacity of corroded steel bridge girders. *Eng. Struct.* **2021**, *238*, 112276. [CrossRef]
7. Khounsida, T.; Nishikawa, T.; Nakamura, S.; Okumatsu, T.; Thepvongsa, K. Study on Static and Dynamic Behavior of Bailey Bridge. In Proceedings of the 2019 World Congress on Advances in Structural Engineering and Mechanics (ASEM19), Jeju Island, Republic of Korea, 17–21 September 2019.

8. Kusimba, B.A.; Rinzin, T.; Banno, Y.; Kinoshita, K. Condition assessment and adaptation of Bailey bridges as a permanent structures. *Appl. Sci.* **2022**, *12*, 11673. [CrossRef]
9. Yi, P.; Vaghela, G.; Buckland, A. Condition Assessment and Load Rating of Arched Bailey Bridge. In Proceedings of the 9th Austroads Bridge Conference, Sydney, New South Wales, Australia, 22–24 October 2014.
10. Biondini, F.; Malerba, P.G. Structural Collapse Analysis of a Bailey Bridge. In *Maintenance, Monitoring, Safety, Risk and Resilience of Bridges and Bridge Networks*; CRC Press: Boca Raton, FL, USA, 2016; p. 407.
11. Fang, Y.; Mitoulis, S.-A.; Boddice, D.; Yu, J.; Ninic, J. Scan-to-BIM-to-Sim: Automated reconstruction of digital and simulation models from point clouds with applications on bridges. *Results Eng.* **2025**, *25*, 104289. [CrossRef]
12. American Association of State Highway and Transportation Officials. *AASHTO LRFD Bridge Design Specifications*, 10th ed.; American Association of State Highway and Transportation Officials: Washington, DC, USA, 2024.
13. Wu, T.; Fan, G.; Dou, C.; Li, X.; Dou, C.; Che, J.; Wang, T.; Rao, J. Simulation study on damage behavior of a shallow-buried Foundation bridge under combined action of flood scouring and heavy vehicle load. *Ocean Eng.* **2025**, *323*, 120410. [CrossRef]
14. Wang, C.S.; Wang, Y.Z.; De Corte, W.; Shu, C. Digital simulation of distortion-induced fatigue in steel bridges with different geometrical configurations. *J. Constr. Steel Res.* **2024**, *216*, 108613. [CrossRef]
15. Shi, X.; Cao, Z.; Ma, H.; Ruan, X. Failure analysis on a curved girder bridge collapse under eccentric heavy vehicles using explicit finite element method: Case study. *J. Bridge Eng.* **2018**, *23*, 05018001. [CrossRef]
16. Xiong, W.; Cai, C.; Kong, B.; Ye, J. Overturning-collapse modeling and safety assessment for bridges supported by single-column piers. *J. Bridge Eng.* **2017**, *22*, 04017084. [CrossRef]
17. Foss, C.F.; Gander, T. *Jane's Military Vehicles and Ground Support Equipment*; Jane's Publishing Company: Croydon, UK, 1981.
18. Praseeda, P.K.; Kamde, D.K.; Basavaraj, A.S.; Sankar, V.; Pillai, R.G. Effect of slag in concrete to enhance service life and reduce carbon footprint of a coastal highway bridge. *Constr. Build. Mater.* **2025**, *489*, 142313. [CrossRef]
19. Wang, Y.; Thrall, A.; Zoli, T. Adjustable module for variable depth steel arch bridges. *J. Constr. Steel Res.* **2016**, *126*, 163–173. [CrossRef]
20. Knight, D.; Brownlie, K.; Marks, J.; McKellar, M.; Boothman, D. Modular by necessity–Bracklinn Falls footbridge. *Proc. Inst. Civ. Eng.-Bridge Eng.* **2024**, *13*, 313–323. [CrossRef]
21. *GB 50017-2017*; Standard for Design of Steel Structures. Ministry of Housing and Urban-Rural Development of PRC: Beijing, China; China Architecture & Building Press: Beijing, China, 2017.
22. *JTG D64-2015*; Specifications for Design of Highway Steel Bridges. Ministry of Transport of PRC: Beijing, China; China Communications Press: Beijing, China, 2015.
23. *GB/T 51232-2016*; Technical Standard for Prefabricated Steel Structure Buildings. Ministry of Housing and Urban-Rural Development of PRC: Beijing, China; China Architecture & Building Press: Beijing, China, 2016.
24. *JTG 3363-2019*; Specifications for Design of Foundation of Highway Bridges and Culverts. Ministry of Transport of PRC: Beijing, China; China Communications Press: Beijing, China, 2019.

Disclaimer/Publisher's Note: The statements, opinions and data contained in all publications are solely those of the individual author(s) and contributor(s) and not of MDPI and/or the editor(s). MDPI and/or the editor(s) disclaim responsibility for any injury to people or property resulting from any ideas, methods, instructions or products referred to in the content.